NeuroImage 222 (2020) 117260

Contents lists available at ScienceDirect

NeuroImage

journal homepage: www.elsevier.com/locate/neuroimage

Structural characterization of the Extended Frontal Aslant Tract trajectory: A ML-validated laterality study in 3T and 7T

Saül Pascual-Diaz[1,*], Federico Varriano[1], Jose Pineda, Alberto Prats-Galino

Laboratory of Surgical Neuroanatomy, Universitat de Barcelona, Spain

ARTICLE INFO

Keywords:
Automated fiber quantification
Extended Frontal Aslant Tract
Lateralization
Machine learning
Dissection
Frontal lobe

ABSTRACT

The Extended Frontal Aslant Tract (exFAT) is a recently described tractography-based extension of the Frontal Aslant Tract connecting Broca's territory to both supplementary and pre-supplementary motor areas, and more anterior prefrontal regions. In this study, we aim to characterize the microstructural properties of the exFAT trajectories as a means to perform a laterality analysis to detect interhemispheric structural differences along the tracts using the Human Connectome Project (HCP) dataset. To that end, the bilateral exFAT was reconstructed for 3T and 7T HCP acquisitions in 120 randomly selected subjects. As a complementary exploration of the exFAT anatomy, we performed a white matter dissection of the exFAT trajectory of two *ex-vivo* left hemispheres that provide a qualitative assessment of the tract profiles. We assessed the lateralization structural differences in the exFAT by performing: (i) a laterality comparison between the mean microstructural diffusion-derived parameters for the exFAT trajectories, (ii) a laterality comparison between the tract profiles obtained by applying the Automated Fiber Quantification (AFQ) algorithm, and (iii) a cross-validated Machine Learning (ML) classifier analysis using single and combined tract profiles parameters for single-subject classification. The mean microstructural diffusion-derived parameter comparison showed statistically significant differences in mean FA values between left and right exFATs in the 3T sample. The diffusion parameters studied with the AFQ technique suggest that the inferiormost half of the exFAT trajectory has a hemispheric-dependent fingerprint of microstructural properties, with an increased measure of tissue hindrance in the orthogonal plane and a decreased measure of orientational dispersion along the main tract direction in the left exFAT compared to the right exFAT. The classification accuracy of the ML models showed a high agreement with the magnitude of those differences.

1. Introduction

The quantitative investigation of the White Matter (WM) connectivity using techniques derived from diffusion imaging, such as tractography, is a powerful approach to the characterization of different tracts in the human brain. However, the high prevalence of crossing fibers in the WM tissue and the geometric complexity of the fiber architecture pose serious limitations to the sensitivity and specificity of the tractographic reconstructions (Jones and Cercignani, 2010).

In order to address this problem, different frameworks of along-tract profiling have been proposed (Chamberland et al., 2019; Corouge et al., 2006; Jones et al., 2005). One of such proposals is the Fiber Quantification Analysis (AFQ) technique (Yeatman et al., 2012), which works by creating a "tract profile" of diffusion measurements at multiple locations along the trajectory of a WM tract. This technique has been successfully applied to investigate several major WM tracts and showed remarkable precision when evaluating the associations between WM properties of different tract profile segments and behavioral outcomes related to normal brain function and diseased states.

In addition, the AFQ technique has been shown to be a robust tool for detecting asymmetries in the human Arcuate Fasciculus across different datasets and pipelines (Bain et al., 2019). Hemispheric asymmetry is a cardinal feature of brain organization and it is known that different areas in the human cerebral cortex are asymmetrical in their structural features (Kong et al., 2018). Asymmetry of WM pathways has also been studied with regards to several cognitive functions, with a paradigmatic example being language, which shows both functional and structural lateralization in the human brain (Bradshaw et al., 2017; Catani et al., 2007; Desmond et al., 1995).

In the frontal lobe territory, a connection between Broca's region (and its contralateral homologous region in the non-dominant hemisphere for language) and the Anterior Supplementary and Pre-Supplementary Motor Areas (SMA and pre-SMA) of the Superior Frontal Gyrus (SFG) has been recently reported in the human brain in dissection

* Corresponding author.
E-mail address: saulpascual@protonmail.com (S. Pascual-Diaz).
[1] These authors contributed equally to this work.

https://doi.org/10.1016/j.neuroimage.2020.117260
Received 10 October 2019; Received in revised form 28 July 2020; Accepted 3 August 2020
Available online 13 August 2020

and tractography studies (Catani et al., 2012): Due to its characteristic slanted trajectory, this tract has been named the Frontal Aslant Tract (FAT). The FAT has been recently included in clinical models of language networks (Dick et al., 2014), it has been suggested that the left FAT serves as a key communicative link between sentence planning and lexical access processes(Chernoff et al., 2018), and evidence shows that loss of integrity of the left FAT is associated with alterations in Primary Progressive Aphasia (PPA) (Catani et al., 2013; Mandelli et al., 2016). An AFQ study showed differences in diffusion measures of the bilateral FAT in persistent developmental stuttering (Kronfeld-Duenias et al., 2014), and its damage is correlated with a loss in speech fluency (Basilakos et al., 2014). Additionally, the FAT has been implicated in visually-oriented hand movements (Budisavljevic et al., 2017).

The initial FAT reconstructions (Catani et al., 2012; 2013) adhere to the SMA and pre-SMA territory parcellation criteria proposed by Picard and Strick (Picard and Strick, 1996; 2001). A commonly used definition for the anterior limit of the pre-SMA region is a virtual line passing through the genu of the *corpus callosum* and parallel to the vertical anterior commissure line (Krainik et al., 2004; Lehéricy et al., 2004). Due to the interindividual variability of the brain and the size of the genu of the *corpus callosum*, this definition has led to many proposals for the FAT reconstruction, some approaching the more restrictive trajectory originally proposed by Catani (Ferpozzi et al., 2018; Vassal et al., 2014), and others offering a wider connection reaching to more anterior regions in the SFG (Rojkova et al., 2016) and, at the same time, suggesting that it could subserve additional cognitive functions beyond language (Dick et al., 2014). In this line, it has been suggested that the FAT could have a potential role for relating hierarchically organized processes outside of language function (Chernoff et al., 2018). Further studies using cytoarchitecture and multimodal approaches have offered additional converging evidence on the spatial location of the pre-SMA in the frontal lobe (Ruan et al., 2018) that agree with the original, relatively more restrictive Catani FAT reconstructions.

In this context, and to address potential ambiguities, we distinguish between the original more restrictive FAT definition, and a wider frontal aslant connection between the sum of *pars opercularis* and *pars triangularis* in the Inferior Frontal Gyrus (IFG), and the totality of the SFG: the extended Frontal Aslant Tract (exFAT). We have shown that bilateral exFAT volume is correlated with language function and the right exFAT volume is correlated with working memory performance in healthy adults (Varriano et al., 2018). The implication of the frontal aslant connections in executive function is an emerging topic in structural neuroimaging research (Dick et al., 2019). In a recent study, we have shown that a clustering procedure using voxel-based morphometry was able to detect two separated clusters with an anterior-posterior relationship in the right exFAT WM trajectory. The posterior component captures fibers from the original FAT trajectory and is related to language (and not working memory) performance, while the anterior component captures fibers from a more anterior frontal aslant component and is related to working memory (and not language) performance (Varriano et al., 2020). The exFAT includes and extends the original FAT definition, and due to its strategic placement reaching more anterior frontal regions, the structural characterization of this connection has the potential to contribute to the understanding of language function, as evidenced by the original FAT results, and to higher-level cognitive functions depending on more anterior connectivity.

The main objective of this study is to characterize the microstructural properties along the exFAT trajectory by calculating a tract profile using the AFQ algorithm as a means to perform a laterality analysis to detect interhemispheric structural differences along the tracts. In addition, we propose a cross-validated Machine Learning (ML) procedure that is capable of performing single-subject inferences by classifying the exFATs into left-right categories according to local microstructural differences along the tract profiles. As a complementary exploration of the exFAT anatomy, we offer the results of a WM dissection of the exFAT trajectory of two *ex-vivo* left hemispheres that provide a qualitative assessment of the underlying anatomy from which the tract profiles are calculated.

Table 1
HCP dataset diffusion acquisition parameters.

	HCP 3T	HCP 7T
Spatial resolution	1.25 mm^3	1.05 mm^3
	LR/RL phase encoding (PE)	AP/PA phase encoding (PE)
Acceleration	Multiband = 3	Multiband = 2
		GRAPPA = 3
	Partial Fourier = 6/8	Partial Fourier = 6/8
Total echo train length	84.24 ms	41 ms
Gradient strength (max)	100 mT/m	70 mT/m
$b-$values(s/mm^2)	1000, 2000, 3000	1000, 2000
Q-space directions	270 × 2	130 × 2

2. Materials and methods

2.1. Human Connectome Project data

This study was performed on neuroimaging data from 120 randomly selected subjects (mean age ± SD of 29.43 ± 3.35 and a male ratio of 0.38) from the WU-Minn 7-tesla Human Connectome Project (HCP) 1200 MRI open-access dataset (http://humanconnectomeproject.org). Three and 7-tesla diffusion-weighted sequences were used. For structural images, 3-tesla T1 sequences were used, as 7-tesla T1 images are not available in the HCP sample.

The 3-tesla HCP acquisition was conducted on a Siemens Magnetom Skyra MRI machine. Structural imaging consisted of a T1 weighted 3D MPRAGE sequence with 224 × 244 mm of FOV with a voxel size of 0.7 mm isotropic (TR = 2400 ms, TE = 2.14 ms, TI = 1000 ms, flip angle of 8 degrees, BW = 210 HZ/Px, iPAT of 2 and the acquisition time was 7 minutes and 40 seconds) (Andersson and Sotiropoulos, 2016). The diffusion-weighted HCP acquisition parameters are summarized in Table 1 (Sotiropoulos et al., 2016; Vu et al., 2015).

According to the HCP consortium, the subjects were healthy individuals that gave written consent to share anonymized brain imaging and behavioral data. The inclusion criteria were the availability of 3T and 7T diffusion data and Freesurfer parcellation data (Fischl et al., 2004).

The HCP subjects have handedness scores according to the Edinburgh Handedness Inventory (EHI). From the 120 subjects of the sample, 107 are right-handed ($50 \leq EHI \leq 100$), 10 are ambidextrous ($-50 < EHI < 50$), and 3 are left-handed ($-100 \leq EHI \leq -50$). The results of this study using the complete sample and the results using only the 107 right-handed subjects were very similar, and because of this, the entire sample of 120 subjects was used for the analyses (Additional figures for the right-handed subsample can be found in Appendix A).

This study was conducted with the approval of the Bioethics Committee of the University of Barcelona, Institutional Review Board (IRB00003099).

2.2. Tractogram reconstructions

For each individual subject, whole-brain tractography reconstructions were performed for the 3T and the 7T diffusion acquisitions with Mrtrix3 (Tournier et al., 2019) software using the iFOD2 (Calamante et al., 2010) algorithm firing randomly distributed seeds in the WM until 10 million streamlines were obtained. Tissue information provided by the Anatomically-Constrained Tractography (ACT) framework (Smith et al., 2012) was used to increase the biological plausibility of the reconstruction, Multi-Shell, Multi-Tissue, Constrained Spherical Deconvolution (MSMT-CSD) (Jeurissen et al., 2014) was performed, and streamlines were cropped at the white/gray matter interface. This allowed us to obtain high-quality tractography reconstruc-

tions and avoid several well-known shortcomings of the tracking procedure (Calamante, 2019).

For each hemisphere, the Desikan-Killiany parcellation (Desikan et al., 2006) from the T1 acquisition in native space was used to obtain the exFAT tractograms from the whole brain tractographic reconstructions by using Broca's region — defined as *Pars Opercularis* and *Pars Triangularis* in the left hemisphere — and its contralateral homologous region in the right hemisphere, and the SFG as inclusion masks (Varriano et al., 2018). Every other gray matter structure other than the two explicitly defined as inclusion ROIs was employed as an exclusion mask to produce automated and robust tract reconstructions while reducing the presence of false-positive tracts (Martínez-Heras et al., 2015). A maximum length limit of 150 mm was defined to reduce the presence of false positives.

2.3. Tract profiles

To obtain the tract diffusion profiles for each oriented exFAT — from SFG to Broca's region (or its contralateral homologous region) — we used the AFQ open source library (https://github.com/yeatmanlab/pyAFQ) implemented in Python software (Van Rossum and Drake, 2012). The AFQ algorithm performs iterative comparisons between fibers to obtain a mean tract trajectory from their distances and lengths in four steps: (i) in the first step each streamline is resampled into 100 equidistant nodes, considering the spread of coordinates as multivariate Gaussian. (ii) Each node contributes to the calculation of the fiber tract core as the average of each *x*, *y*, and *z* coordinates, and the spread of fibers is calculated by computing the covariance between nodes. (iii) Each node is represented as a mean coordinate value, *m*, and by a 3 × 3 covariance matrix. For each of these matrices the AFQ algorithm calculates its Mahalanobis distance, $D_m(x)$ as follows:

$$D_m(r) = \sqrt{(r-\mu)^T S^{-1}(r-\mu)^T},$$

where *r* is a vector containing the fiber node's *x*, *y*, and *z* coordinates. (iv) All the fibers that are more than 5 standard deviations away from the core of the fiber tract or more than 4 standard deviations away from the mean fiber length are removed. Steps i–iv are iterated until no outliers remain (Yeatman et al., 2012).

The resulting 100 equidistant nodes can be interpolated with a value for each diffusion-derived parameter — Fractional Anisotropy (FA), Mean Diffusivity (MD), Radial Diffusivity (RD) and Axial Diffusivity (AD) — across each of the nodes along the exFAT streamlines (Bain et al., 2019). Diffusion-derived parameters were calculated using the tensor2map (Basser et al., 1994) tool from the Mrtrix3 package.

2.4. Statistical analyses

As a preliminary and general overview of the dataset, we perform a global analysis in which mean values (and standard deviations) were calculated for each microstructural diffusion-derived parameter in each tract. A laterality test was performed using t-tests to compare left and right mean exFAT microstructural diffusion-derived parameters. Cohen's *d* was used to evaluate the effect size of the significant results using the expression:

$$d = \frac{\sqrt{2}(\bar{x_1} - \bar{x_2})}{\sqrt{(SD)_1^2 + (SD)_2^2}}.$$

In the AFQ analysis, we calculated a Laterality Index (LI) for each node of the left and right exFAT tract profiles using the expression:

$$LI = \frac{V_{left} - V_{right}}{V_{left} + V_{right}}.$$

Where *V* is the specific map value (FA, MD, RD or AD) for each coordinate in the left and right exFAT tract profile. Each pair of nodes was compared using a t-test.

Table 2
Mean values for the diffusion-derived microstructural parameters.

	FA	MD	RD	AD
3T left	0.451 ± 0.016	0.538 ± 0.017	0.399 ± 0.016	0.816 ± 0.024
3T right	0.440 ± 0.017	0.538 ± 0.016	0.404 ± 0.016	0.808 ± 0.023
7T left	0.467 ± 0.018	0.589 ± 0.020	0.430 ± 0.021	0.907 ± 0.024
7T right	0.465 ± 0.017	0.589 ± 0.021	0.430 ± 0.020	0.905 ± 0.024

All the t-tests were calculated after performing a Shapiro-Wilk test to confirm normality and an F test to prove homoscedasticity. The resulting p-values were corrected for multiple comparisons using the Bonferroni correction if applicable ($p < \alpha$). A total of 808 comparisons were made in this study, 8 comparisons in global analyses and 800 in the AFQ corresponding of 100 nodes × 4 metrics × 2 fields. The null hypothesis, H_0, was rejected for corrected p-values ($p \times 808$, being 1 the upper bound) under our significance threshold established at $\alpha = 0.05$. The MD, RD, and AD maps were multiplied by 1K for scaling convenience. All statistical tests were performed using Python software.

2.5. Machine learning model

In order to validate the laterality indices differences in the resulting tract profiles and make inferences at the single-subject level, we developed an ML-model. We ran a repeated random sub-sampling cross-validated procedure based on a regularized logistic regression classifier using sklearn (Pedregosa et al., 2012) with a testing/training split ratio of 0.3, Limited-Memory Broyden–Fletcher–Goldfarb–Shanno (L-BFGS) solver and L2 penalty. The ML classification algorithm was trained with separate data from FA, MD, RD, and AD values derived from the zs-cored tract profiles and with a vector combining every diffusion parameter. The training/testing procedure was repeated 10K times in order to ensure the robustness of the ML classification algorithm under random permutations of the results dataset.

2.6. White matter fiber dissection

Two left human brain hemispheres were obtained within the first 24 h post mortem from donors with no clinical history of neurological disease. After inspecting the brains for any abnormalities, the specimens were prepared in accordance with Klingler's method (Klingler and Ludwig, 1956). The specimens were fixated in a 10% formaldehyde solution for 2 months. Each hemisphere was frozen at −16°C for 2 weeks. The arachnoid and *pia mater* of each hemisphere were removed after thawing the specimens under tap water for 24 hours. The fiber dissections of the brain hemispheres were performed in a stepwise manner, from lateral to medial.

3. Results

3.1. Descriptive results

The mean values for the different diffusion parameters and MRI fields for the bilateral exFAT territories can be seen in Table 2.

For more detailed information about the exFAT trajectory, an additional figure showing the probabilistic map for all the sample at both 3T and 7T can be found in Appendix B.

3.2. Laterality results

In the mean microstructural diffusion-derived parameters comparison, we found statistically significant differences between left and right FA values ($p < 0.001$) with a medium–large effect size of 0.648 for the 3T data. We did not find left/right differences in diffusion-derived parameters for the 7T data. The results are shown in Table 3 (additional violin plot shown in Appendix C).

Table 3
Laterality comparison between the mean microstructural diffusion-derived parameters for the exFAT trajectories. † indicates Bonferroni corrected *p*-values. * Indicates H_0 rejection at Bonferroni corrected p-values.

	FA			MD			RD			AD		
	t-val	*p*-val	*d*-val	*t*-val	*p*-val	*d*-val	*t*-val	*p*-val	*d*-val	*t*-val	*p*-val	*d*-val
3T	5.356	< 0.001†*	0.648	−0.086	0.932	–	−2.293	1†	–	2.890	1†	–
7T	0.801	0.424	–	0.016	0.987	–	−0.285	0.775	–	0.516	0.606	–

Table 4
Significant segments of the tract profile for the 3T and 7T AFQ analyses.

	3T				7T			
	Segment	AUC	Max *p*-value	Laterality	Segment	AUC	Max *p*-value	Laterality
FA	[37, 100] (64%)	1.828	0.029	Left	[72, 78] (7%)	0.117	0.031	Left
MD	[65, 78] (14%)	0.180	0.043	Right	–	–	–	–
RD	[57, 96] (40%)	1.035	0.030	Right	—	—	—	—
AD	[93, 100] (8%)	0.117	0.036	Left	[68, 77] (9%)	0.118	0.041	Left

Table 5
Table showing the accuracy results of the laterality ML classifiers for the different microstructural parameters and for each field. Values correspond to mean accuracies ± standard deviation for the 10K iterations of the cross-validated models.

	FA	MD	RD	AD	Combined model
3T	0.890 ± 0.042	0.793 ± 0.053	0.889 ± 0.041	0.670 ± 0.061	0.911 ± 0.040
7T	0.660 ± 0.061	0.629 ± 0.063	0.618 ± 0.063	0.719 ± 0.059	0.768 ± 0.059

In the AFQ laterality comparison, we report the significant segments along the tract profile together with its percentile position, the Area Under the Curve (AUC), the maximum Bonferroni-corrected significant *p*-value, and its asymmetry value for the laterality analysis in Table 4 and Fig. 1.

For the 3T AFQ laterality analyses we found a left lateralization pattern for the FA and AD tract profiles and a right lateralization pattern for the MD and RD tract profiles. For the 7T AFQ laterality analyses we found a left lateralization pattern for the FA and AD tract profiles and no laterality differences were found for the MD and RD tract profiles.

3.3. Machine Learning model

Accuracies of the ML models for single-subject classification of AFQ exFAT profiles can be seen in Table 5 for the laterality analyses (Additional figures, confusion matrices and comparisons with a random classifier can be found in Appendix D).

3.4. White matter dissection

In the WM dissection study performed on two left hemispheres, we revealed the exFAT trajectory using a stepwise procedure and obtained two oblique coronal slices that approximate the plane of the AFQ tract profile. In those slices, we distinguish three anatomically different regions along the exFAT trajectory as shown in Fig. 2 (an additional picture of the specimen shown in Fig. 2(a) before the slicing can be seen in Appendix E).

4. Discussion

4.1. Laterality analysis

In the present work, we performed a laterality study by comparing tract profiles along the exFAT trajectory. The systematic reconstruction of the exFAT provides a reproducible way of reconstructing the frontal aslant connectivity beyond the pre-SMA — as originally defined by Picard and Strick (Picard and Strick, 1996; 2001) — explicitly addressing the problem of FAT reconstructions reaching to more anterior frontal cortical regions.

Overall, the global analysis did not detect laterality differences for the average microstructural properties of the exFAT, with the exception of the FA values, which showed a significant left lateralization pattern in the 3T acquisitions, but not in the 7T acquisitions.

The AFQ analysis provided additional and in-depth information for the microstructural properties along different segments of the exFAT tract profile, offering insights regarding its laterality properties beyond what can be seen in the global analysis. We have detected significant laterality differences along the exFAT tract profiles for all the measured microstructural parameters in the 3T field, and for FA and AD parameters in the 7T field. All the significant segments were detected in the inferiormost 60% of the exFAT tract profiles. The FA tract profile comparisons show an exclusive left lateralization pattern of the significant segments for both 3T and 7T fields. This is compatible with results from Bain et al. (2019) where laterality comparisons of tract profiles of the arcuate fasciculus showed a left lateralization pattern of FA values in the regions approaching Broca's territory.

For the 7T field, where the global analysis failed to detect differences, we can distinguish significant left-lateralized segments for the FA and the AD tract profiles when approaching the IFG. Nevertheless, the 3T data was capable of a better characterization of the laterality properties of the exFAT trajectory compared to the 7T data: the cumulative AUC corresponding to statistically significant segments in the 3T field was around 17 times higher than in the 7T data. One reasonable explanation for the increased sensitivity of the exFAT AFQ laterality analyses in the 3T data, as seen by its higher AUC values, is that there is a trade-off between 3T and 7T HCP datasets, where the 3T HCP dataset has a lower spatial resolution, but it contains an additional third shell of higher *b*-value ($b = 3000$ s/mm^2) that allows for a wider sampling of the *q*-space (Vu et al., 2015). Under these circumstances, the MSMT-CSD algorithm is capable of resolving more complex fiber crossing patterns in the 3T data (Sotiropoulos et al., 2013) and this additional

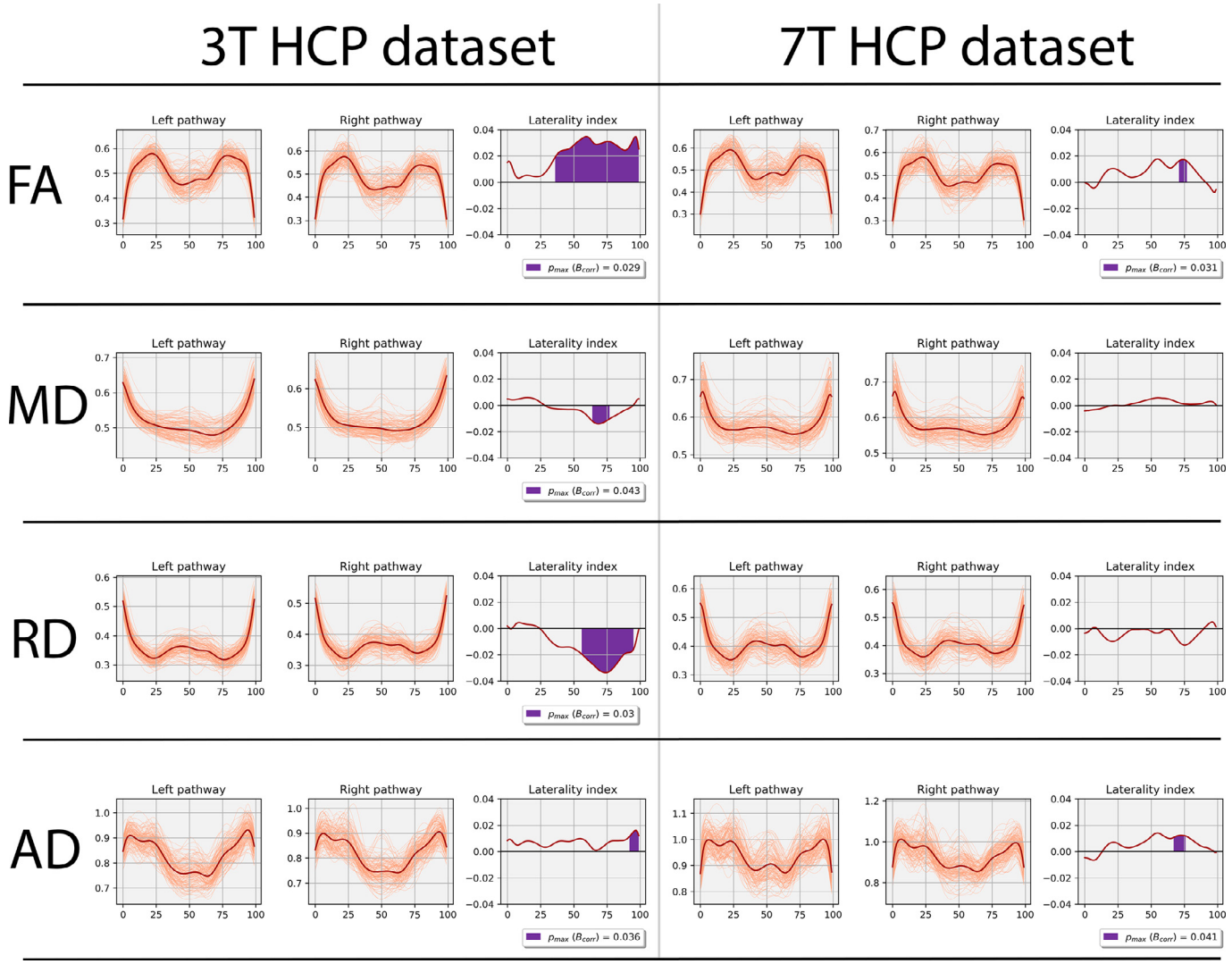

Fig. 1. AFQ tract profiles oriented from the SFG to Broca's region (or its contralateral homologous region) — superior (1) ↔ inferior (100) — for each diffusion-derived microstructural parameter. Significant centiles after Bonferroni correction in the laterality index analysis are shown in purple. Individual tract profiles are shown in salmon color and the mean tract profile is shown in red.

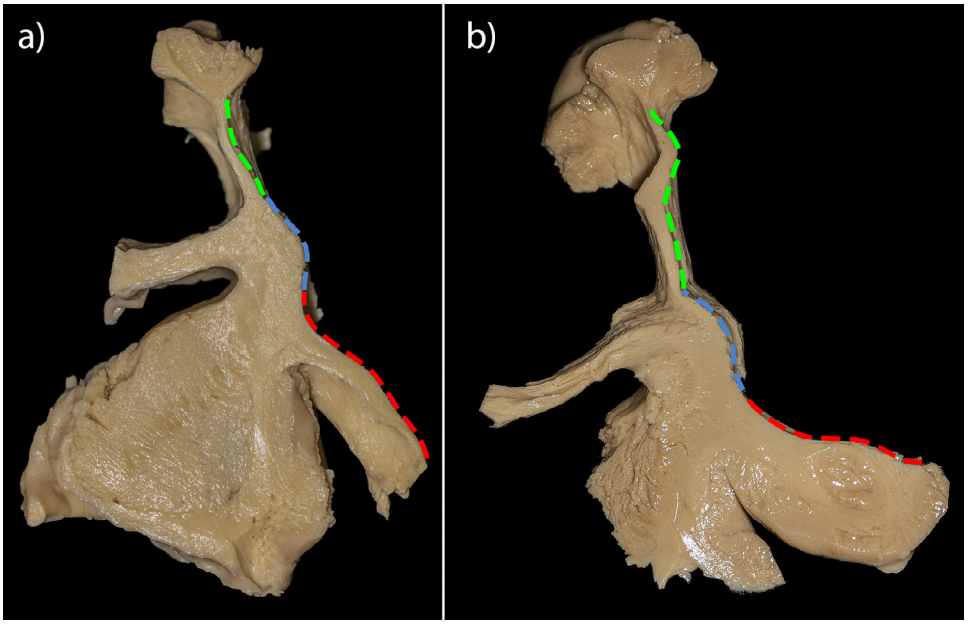

Fig. 2. Coronal slices of two dissected left hemispheres showing the central region of the exFAT trajectory. Colored dashed lines highlight anatomically distinguishable segments: in green, the trajectory from SFG to the central convex region. In blue, the central convex region. In red, from the central convex region to the IFG.

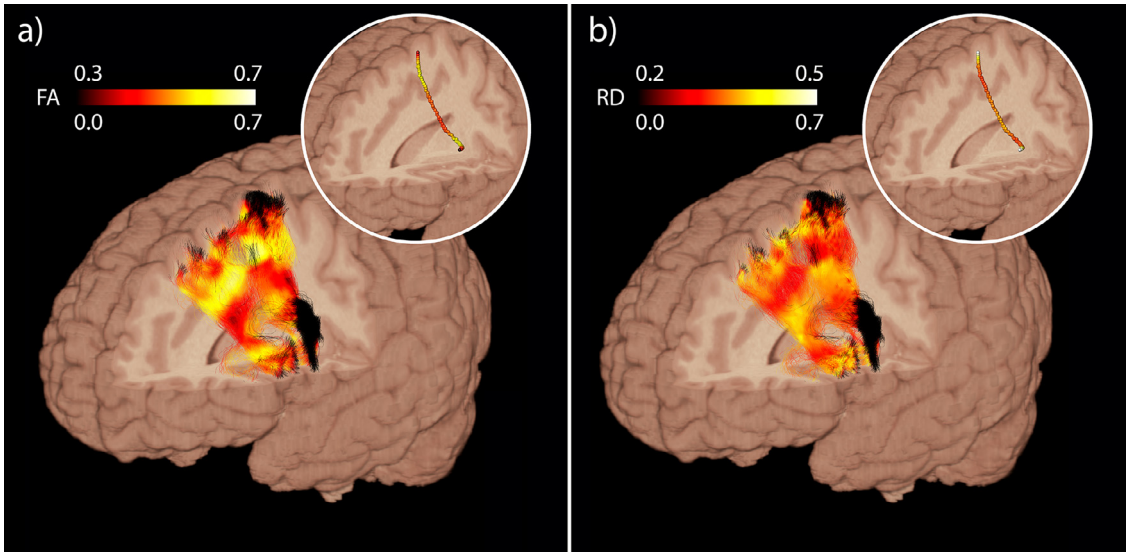

Fig. 3. Lateral view of an exFAT reconstruction in the left hemisphere with (a) FA values projected along the fiber trajectories with a lateral view of the FA tract profile, and (b) RD values projected along the fiber trajectories with a lateral view of the RD tract profile. The colormap scale indicates the relative value intensity for each corresponding microstructural parameter. Maximum and minimum values for the parameters projected over the exFAT fiber core and the exFAT fibers are respectively shown above and below the scale color bar.

resolution could positively impact the reconstruction of the AFQ tract profiles.

The ML classifiers were able to perform single-subject laterality classification on the testing datasets with very high accuracy, showing that the average microstructure differences, as detected in the AFQ analysis, correspond to single-subject-level patterns of lateralization along the exFAT trajectory. In the 3T ML classification algorithms, FA and RD were the parameters leading to the highest classification accuracy (89.0 ± 4.2% for the FA and 88.9 ± 4.1% for the RD) while AD led to the lowest (67.0 ± 6.1%). The ML models performed better in 3T than in 7T. The combined ML model offered a marginal improvement in classification accuracy (91.1% ± 4.0%) compared to the best-performing single-parameter models. This suggests that an accurate profile fingerprint can be extracted from a subset of microstructural parameters measured along the tract. This is compatible with dimensionality reduction studies showing that models of combined microstructural parameters can be effectively reduced, with minor losses of explained variance, to two biologically interpretable components, one related to orientational dispersion, and the other related to hindrance restrictions in tissue microstructure (Chamberland et al., 2019). To this regard, our results show a significantly higher diffusion hindrance and a lower orientational dispersion in the central and inferiormost parts of the left exFAT trajectory compared to the right exFAT trajectory.

Overall, the AFQ laterality analyses were capable of detecting significant differences along the tract profiles, with overlapping segments where significant differences were present for more than one microstructural diffusion-derived parameter. The ML results strongly agree with the AFQ results, as the ML classifiers showed a very good performance in cases where the AFQ AUC was high. Moreover, in cases where the AFQ AUC was small or 0, the ML classifiers were still able to detect additional nonlinearities which allowed them to perform single-subject classification with higher-than-chance accuracy.

4.2. exFAT trajectory characterization

For both the 3T and 7T fields, the average AFQ tract profiles show a marked decrease around the central percentiles of the trajectory in the FA and AD values. The RD values, which tend to be inversely correlated to AD values in coherently organized WM bundles, show an inverse behavior along the tract profiles, while the MD values show a flatter profile. A single-subject case with tract profile values for FA and RD projected onto the exFAT fibers can be seen in Fig. 3.

The stepwise procedure of the exFAT dissection required extreme care when approaching the lateral surface of the frontal lobe after the removal of the U-fibers, as the Superior Longitudinal Fascicle fibers run anteroposteriorly forming a sheet that closely embraces a large part of the aslant fibers. The results shown in the WM dissection of the exFAT are compatible with what was observed in the AFQ analyses, which showed differences in the central region of the AFQ tract profiles compared to the extremes: although the dissection of the exFAT extremes (red and green segments in Fig. 2) is facilitated by the presence of smooth parallel fibers along the tract direction (and thus we would expect a high FA and a low RD), the dissection of the central region, which describes a convex shape (blue segments in Fig. 2), is particularly challenging due to the high prevalence of crossing fibers (and thus we would expect a low FA and a high RD). Even though the dissection study is of complementary and qualitative nature, it offers a strong ground truth validation that allows us to reject high-level reconstructions that explicitly disagree with its results (e.g. should the dissection study have revealed a pattern of crossing fibers in the distal parts of the exFAT that was not reflected in the properties of the AFQ tract profiles, we could not accept the validity of the tract profiles for the exFAT characterization).

Previous studies have reported that the Fronto-Striatal Tract (FST) could be a fiber population that crosses the central region of the frontal aslant connections (Dick et al., 2019; Kinoshita et al., 2014). We show that the central region of the exFAT is a densely transversed area where coherently organized fibers connecting the Middle Frontal Gyrus (MFG) through the FST, the thalamocortical radiations, and MFG–MFG commissural connections from the anterior region of the *corpus callosum* lead to a high level of intra-voxel fiber crossing. This situation is represented for a single subject in Fig. 4.

Crucially, the results obtained from the exFAT AFQ laterality analyses and the complementary results obtained from the exFAT WM dissection studies offer converging evidence for the existence of a central region of crossing fibers and two extreme segments of higher diffusion hindrance and lower orientational dispersion.

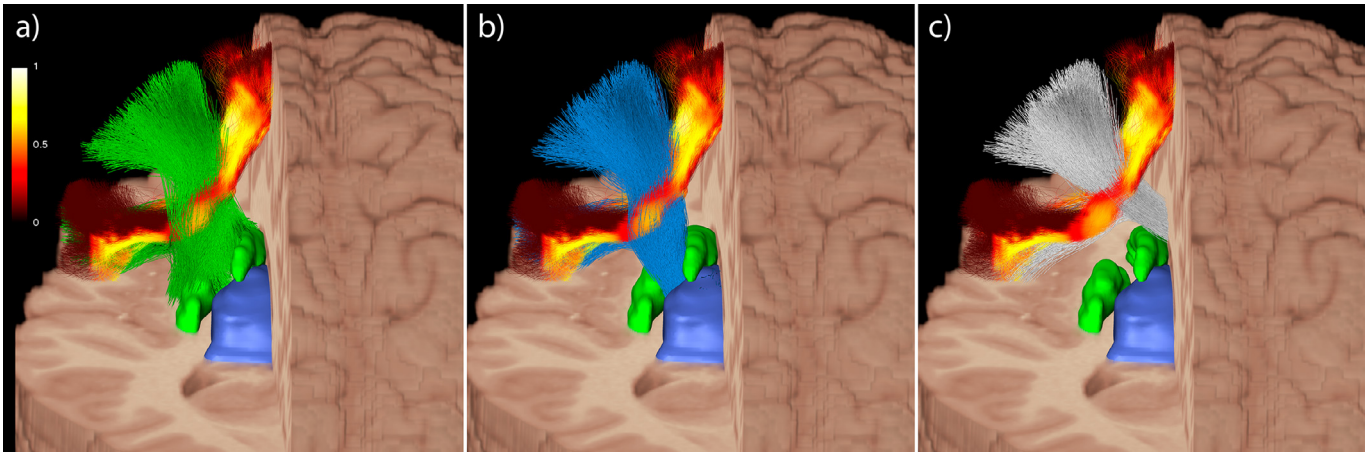

Fig. 4. Single-subject tractography reconstruction showing the high prevalence of crossing fibers along the central convex region of the left exFAT. A volumetric render of the left *striatum* and *thalamus* can be seen in green and blue colors respectively. (a) The fronto-striatal fibers connecting to MFG and the IFG are shown in green. (b) The thalamocortical radiations connecting to MFG and the IFG are shown in blue. (c) The MFG–MFG and the MFG–IFG commissural fibers are shown in white. The FA values have been projected to the exFAT fibers. The colormap scale indicates the FA values for the exFAT.

5. Limitations

The AFQ analysis projects the tract trajectory along the main tract direction. This means that differences present along the direction of the fibers can be detected, while differences existing in the perpendicular plane (e.g. the possibility that the exFAT could contain distinct anterior and posterior components) would be averaged out. Furthermore, the AFQ analysis collapses the complexity of the entire tract in the representation of the tract profile. While this is a powerful and useful approach, complementary methods are necessary for an in-depth exploration of the totality of the tract and to characterize heterogeneous regions distant from the fiber core.

Even though the dissected hemispheres offer complementary evidence for the tractography reconstructions, it must be noted that the number of dissected hemispheres is low, and lack right-hemisphere specimens and MRI acquisitions that could provide same-subject comparisons between dissection data and diffusion data, as *ex vivo* diffusion MRI is still, to our best knowledge, an open problem with additional challenges.

Bridging the gap between structural properties of brain connections and human behavior is a complex and open question. Here, we studied the exFAT trajectory and its laterality differences from a structural perspective, which should be complemented by studies approaching its functional and behavioral implications.

In order to better characterize the implication of the exFAT in human behavior, functional studies characterizing the cortical regions connected by the exFAT fibers should be performed. Furthermore, the functional interplay between the frontal aslant connectivity and the frontal lobe U-fibers should be studied. In addition, and to better understand the differences between the 3T results and the 7T results, further studies should be conducted to understand the effects of data resolution on the structural properties of the exFAT.

6. Conclusions

We have performed a characterization of the microstructural properties along the exFAT trajectory using the AFQ technique in 3T and 7T acquisitions. After applying a conservative multiple comparison correction, we have found significant lateralization differences for diffusion-derived microstructural parameters in the central and inferior regions of the exFAT in the 3T sample (FA, MD, RD, and AD) and in the 7T sample (FA and AD). The average AFQ tract profiles show a marked decrease around the central percentiles of the trajectory in the FA and AD values together with an increase of RD values suggesting the presence of a central region of crossing fibers. These results show that a hemisphere-dependant fingerprint can be obtained from a subset of microstructural parameters measured along the exFAT, as shown by a cross-validated ML classifier model that was capable of detecting laterality differences by performing left-right classification with a high accuracy. As a complementary exploration of the exFAT anatomy, we performed a white matter dissection study of the exFAT trajectory that offered converging evidence for the presence of a central region of crossing fibers and two extreme segments of higher diffusion hindrance and lower orientational dispersion.

Declaration of Competing Interest

The authors declare no conflict of interest. This research did not receive any specific grant from funding agencies in the public, commercial, or not-for-profit sectors.

CRediT authorship contribution statement

Saül Pascual-Diaz: Conceptualization, Data curation, Formal analysis, Investigation, Methodology, Software, Visualization, Writing - original draft, Writing - review & editing. **Federico Varriano:** Conceptualization, Data curation, Formal analysis, Investigation, Methodology, Software, Visualization, Writing - original draft, Writing - review & editing. **Jose Pineda:** Investigation, Visualization, Writing - review & editing. **Alberto Prats-Galino:** Investigation, Project administration, Resources, Supervision, Validation, Visualization, Writing - review & editing.

Acknowledgments

We are grateful to the WU-Minn Consortium for the open release of the Human Connectome Project, without which this project would not have been possible.

Appendix A. Right-handed results

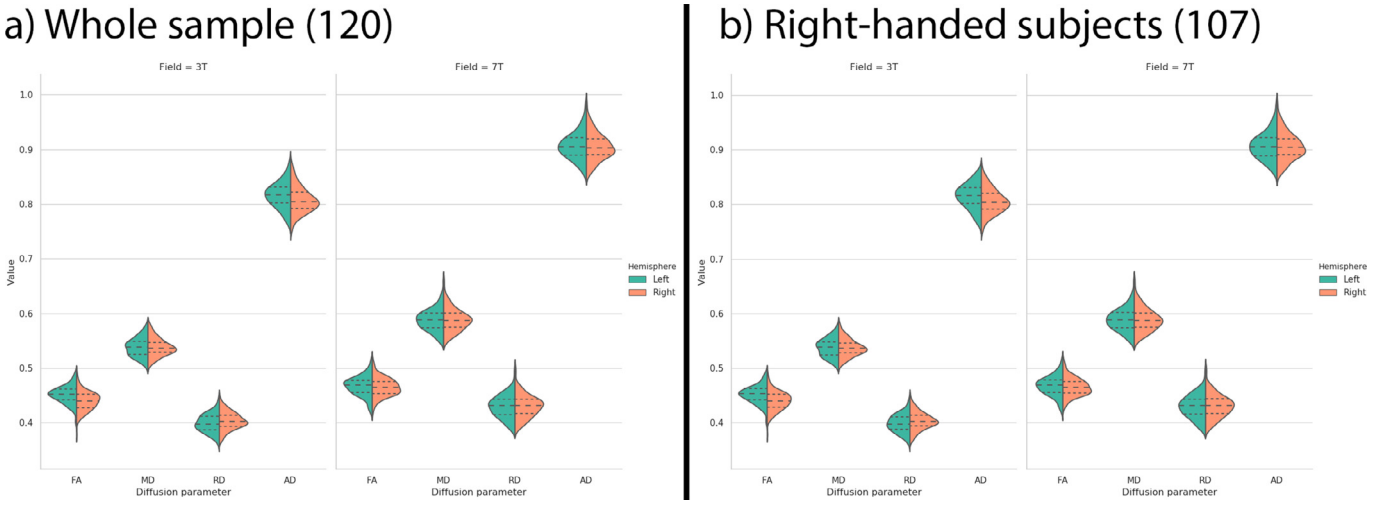

Fig. A1. Violin plots representing the left/right distribution of diffusion-derived microstructural parameters for each field for the whole-sample and for the right-handed subjects. Quartiles are shown in dashed lines. In this figure we illustrate that the mean values for the diffusion-derived microstructural parameters of the exFAT are similar across handedness.

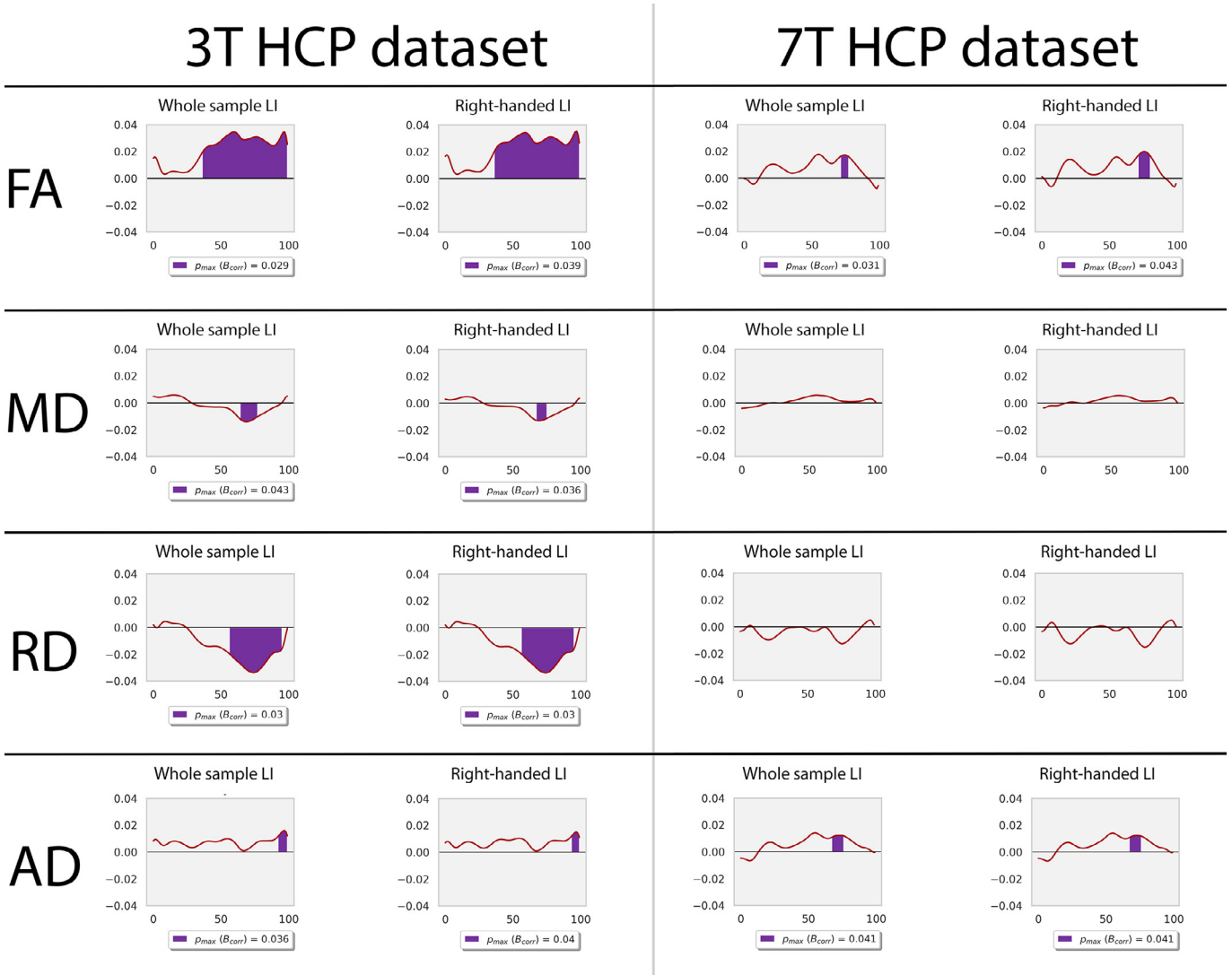

Fig. A2. Laterality indices for the AFQ analyses oriented from the SFG to Broca's region (or its contralateral homologous region) — superior (1) ↔ inferior (100) — for the whole sample and for the right-handed sample. In this figure we illustrate that the tract profiles of the exFAT are similar across handedness.

Appendix B. exFATs probabilistic maps for the 120 subjects.

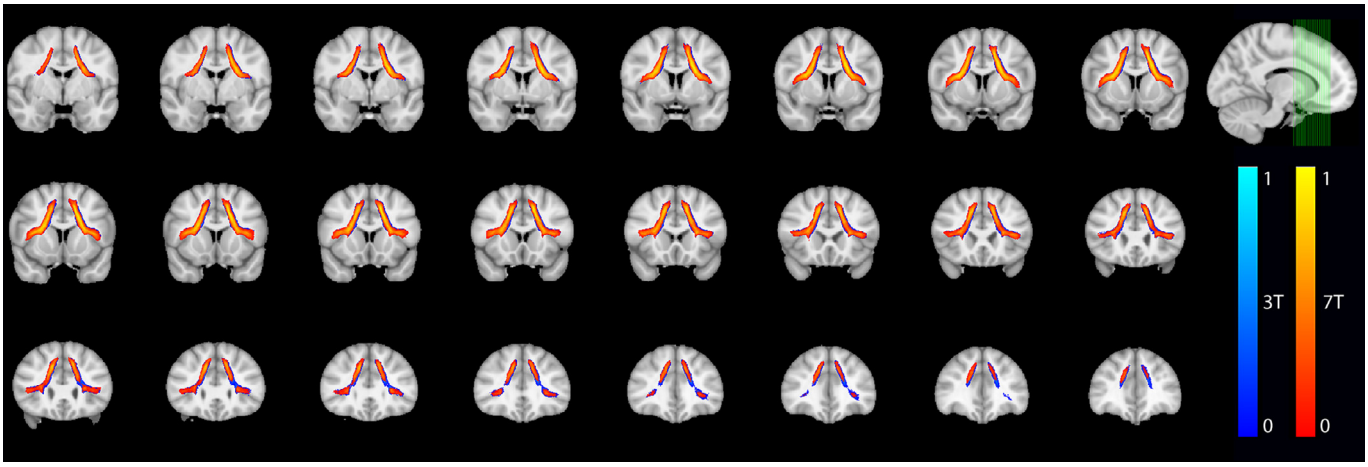

Fig. B1. Probabilistic maps of the exFATs. 3T density maps shown in red-yellow colormap, 7T density maps shown in blue colormap. The calculated overlap for the 3T-7T intersection is 79.9% with the 3T exFATs and 96.4% with the 7T exFATs. A threshold of 50% has been applied.

Appendix C. Violinplot for the global laterality comparisons.

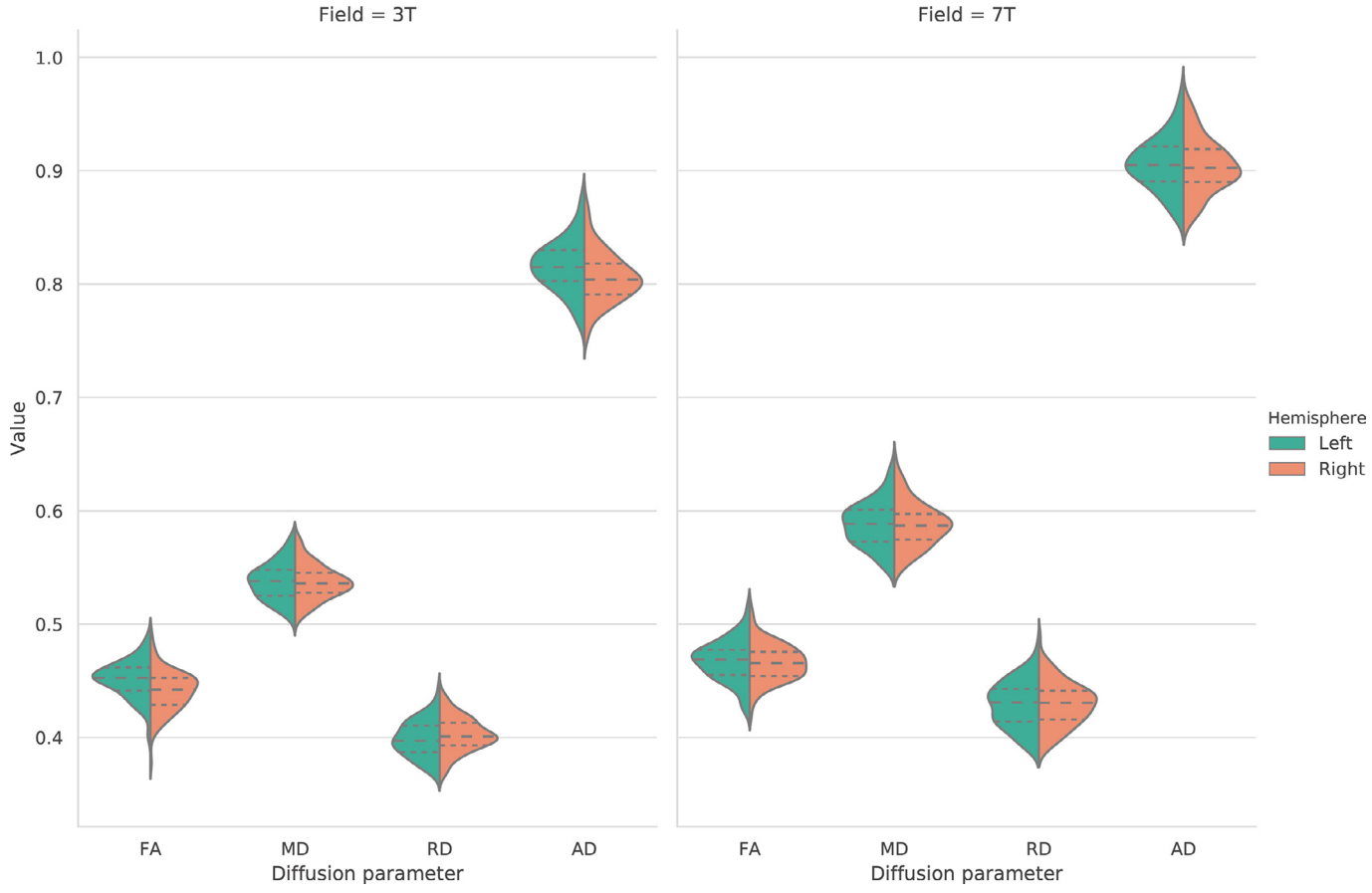

Fig. C1. Violin plots representing the left/right distribution of diffusion-derived microstructural parameters for each field. Quartiles are shown in dashed lines.

Appendix D. Machine Learning confusion matrices

a)

	True left	True Right
Left labeled	110.701 ± 1.685	8.366 ± 1.896
Right labeled	9.299 ± 1.685	111.634 ± 1.896

b)

	True left	True Right
Left labeled	99.308 ± 2.415	20.207 ± 2.619
Right labeled	20.692 ± 2.415	99.730 ± 2.619

c)

	True left	True Right
Left labeled	110.000 ± 1.872	9.907 ± 1.525
Right labeled	10.000 ± 1.872	110.093 ± 1.525

d)

	True left	True Right
Left labeled	88.190 ± 3.287	34.111 ± 3.483
Right labeled	31.810 ± 3.287	85.889 ± 3.483

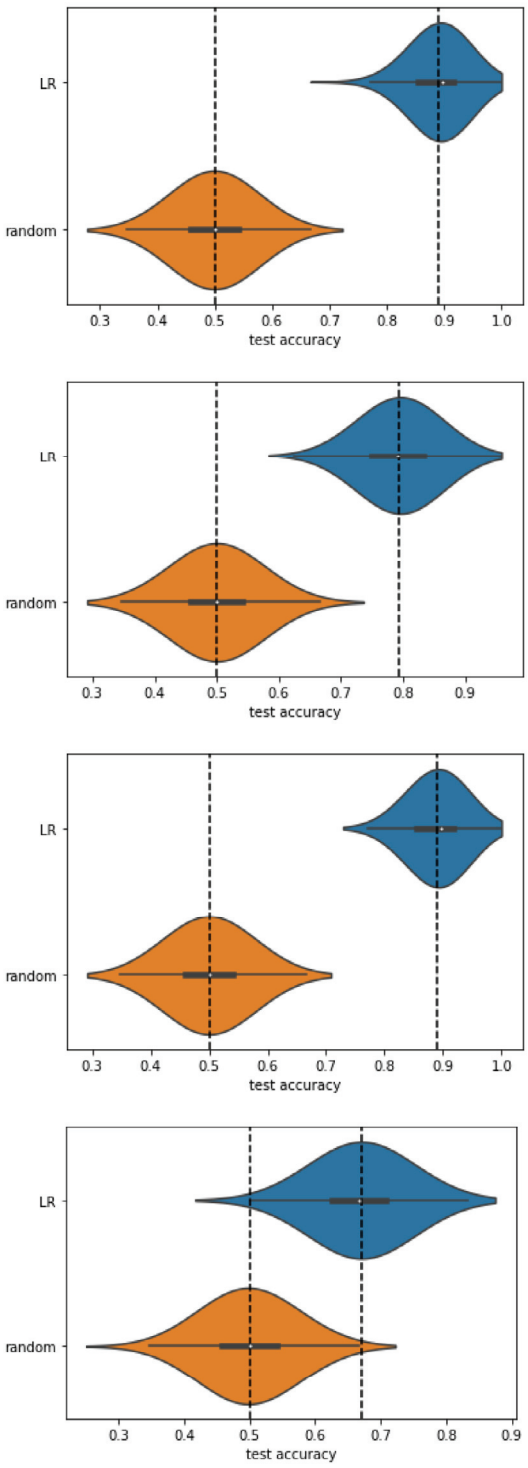

Fig. D1. Confusion matrices for the ML models for the laterality classification of the (a) FA, (b) MD, (c) RD and (d)AD at 3T. Violin plot of the logistic regressor classifier accuracy (blue) compared with a random classifier (orange).

a)

	True left	True Right
Left labeled	86.562 ± 3.494	33.550 ± 3.257
Right labeled	33.438 ± 3.494	86.450 ± 3.257

b)

	True left	True Right
Left labeled	81.993 ± 4.785	35.032 ± 4.321
Right labeled	38.004 ± 4.785	84.968 ± 4.321

c)

	True left	True Right
Left labeled	82.446 ± 4.526	34.428 ± 4.673
Right labeled	37.554 ± 4.526	85.572 ± 4.673

d)

	True left	True Right
Left labeled	94.301 ± 2.883	27.587 ± 3.796
Right labeled	25.699 ± 2.883	92.413 ± 3.796

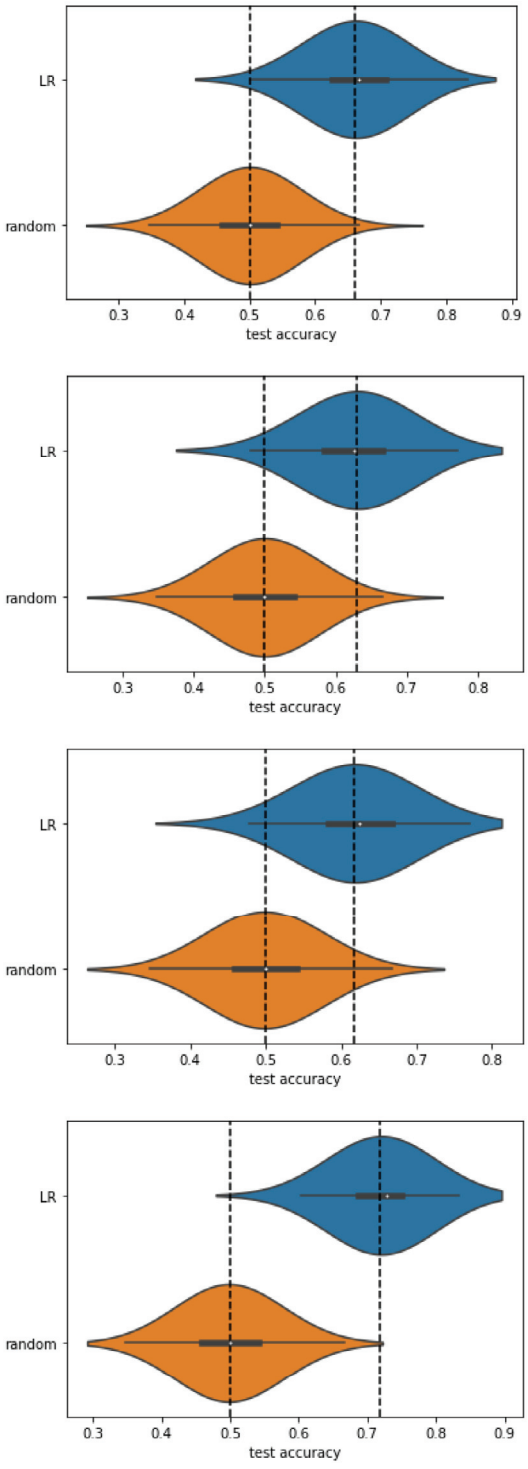

Fig. D2. Confusion matrices for the ML models for the laterality classification of the (a) FA, (b) MD, (c) RD and (d)AD at 7T. Violin plot of the logistic regressor classifier accuracy (blue) compared with a random classifier (orange).

Appendix E. Dissected exFAT trajectory.

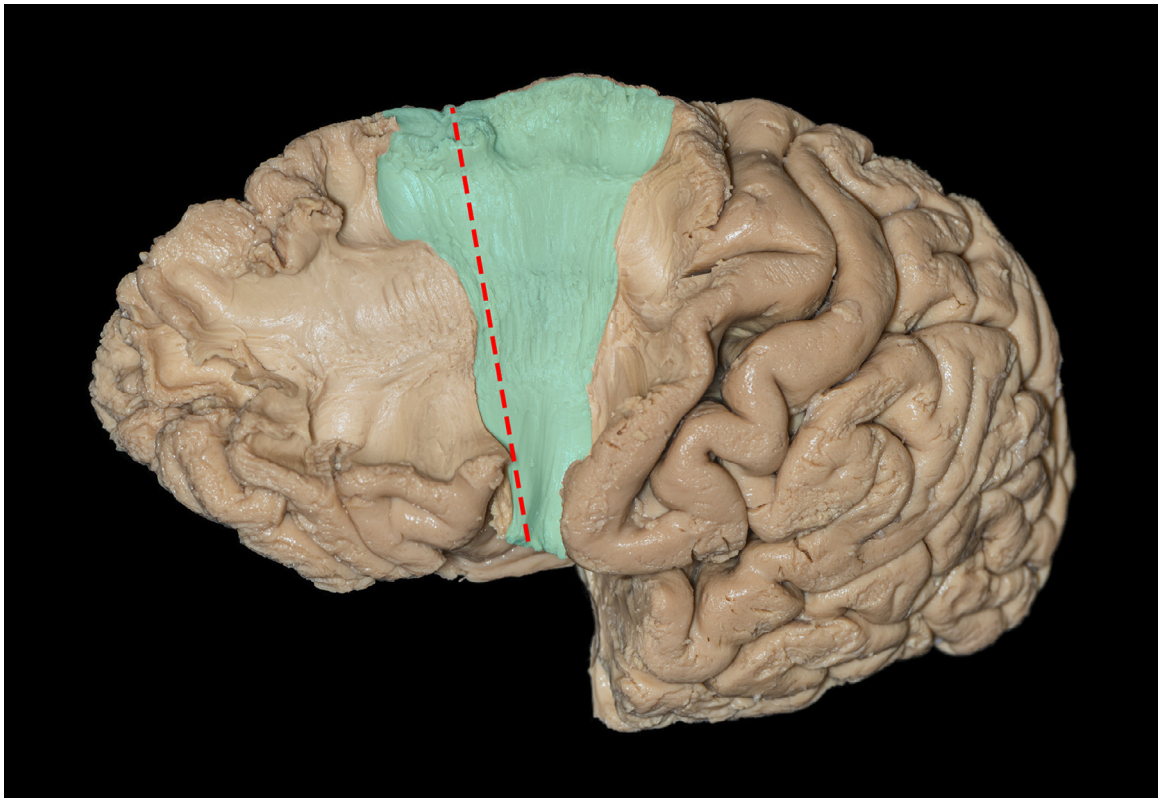

Fig. E1. Lateral view of a dissected hemisphere revealing the exFAT trajectory. The red dashed line indicates the slicing location corresponding to Fig. 2(a) and approximates the spatial location of the AFQ tract profile.

Supplementary material

Supplementary material associated with this article can be found, in the online version, at 10.1016/j.neuroimage.2020.117260

References

Andersson, J.L.R., Sotiropoulos, S.N., 2016. An integrated approach to correction for off-resonance effects and subject movement in diffusion MR imaging. NeuroImage 125, 1063–1078. doi:10.1016/j.neuroimage.2015.10.019.

Bain, J.S., Yeatman, J.D., Schurr, R., Rokem, A., Mezer, A.A., 2019. Evaluating arcuate fasciculus laterality measurements across dataset and tractography pipelines. Hum. Brain Mapp. (May) hbm.24626. doi:10.1002/hbm.24626.

Basilakos, A., Fillmore, P.T., Rorden, C., Guo, D., Bonilha, L., Fridriksson, J., 2014. Regional white matter damage predicts speech fluency in chronic post-stroke aphasia. Front. Hum. Neurosci. 8 (October), 845. doi:10.3389/fnhum.2014.00845.

Basser, P.J., Mattiello, J., LeBihan, D., 1994. MR diffusion tensor spectroscopy and imaging. Biophys. J. 66 (1), 259–267. doi:10.1016/S0006-3495(94)80775-1.

Bradshaw, A.R., Bishop, D.V., Woodhead, Z.V., 2017. Methodological considerations in assessment of language lateralisation with fMRI: a systematic review. PeerJ 2017 (7). doi:10.7717/peerj.3557.

Budisavljevic, S., Dell'Acqua, F., Djordjilovic, V., Miotto, D., Motta, R., Castiello, U., 2017. The role of the frontal aslant tract and premotor connections in visually guided hand movements.. NeuroImage 146 (April 2016), 419–428. doi:10.1016/j.neuroimage.2016.10.051.

Calamante, F., 2019. The seven deadly sins of measuring brain structural connectivity using diffusion MRI streamlines fibre-tracking. Diagnostics 9 (3), 115. doi:10.3390/diagnostics9030115.

Calamante, F., Tournier, J.-D., Connelly, A., 2010. Improved probabilistic streamlines tractography by 2 nd order integration over fibre orientation distributions. Ismrm 88 (2003), 2010.

Catani, M., Allin, M.P.G., Husain, M., Pugliese, L., Mesulam, M.M., Murray, R.M., Jones, D.K., 2007. Symmetries in human brain language pathways correlate with verbal recall. Proc. Natl. Acad. Sci. 104 (43), 17163–17168. doi:10.1073/pnas.0702116104.

Catani, M., Dell'Acqua, F., Vergani, F., Malik, F., Hodge, H., Roy, P., Valabregue, R., Thiebaut de Schotten, M., 2012. Short frontal lobe connections of the human brain. Cortex 48 (2), 273–291. doi:10.1016/j.cortex.2011.12.001.

Catani, M., Mesulam, M.M., Jakobsen, E., Malik, F., Martersteck, A., Wieneke, C., Thompson, C.K., Thiebaut De Schotten, M., Dell'Acqua, F., Weintraub, S., Rogalski, E., 2013. A novel frontal pathway underlies verbal fluency in primary progressive aphasia. Brain 136 (8), 2619–2628. doi:10.1093/brain/awt163.

Chamberland, M., Raven, E.P., Genc, S., Duffy, K., Descoteaux, M., Parker, G.D., Tax, C.M., Jones, D.K., 2019. Dimensionality reduction of diffusion MRI measures for improved tractometry of the human brain. NeuroImage 200 (June), 89–100. doi:10.1016/j.neuroimage.2019.06.020.

Chernoff, B.L., Teghipco, A., Garcea, F.E., Sims, M.H., Paul, D.A., Tivarus, M.E., Smith, S.O., Pilcher, W.H., Mahon, B.Z., 2018. A role for the frontal aslant tract in speech planning: a neurosurgical case study. J. Cogn. Neurosci. 30 (5), 752–769. doi:10.1162/jocn_a_01244.

Corouge, I., Fletcher, P.T., Joshi, S., Gouttard, S., Gerig, G., 2006. Fiber tract-oriented statistics for quantitative diffusion tensor MRI analysis. Medical Image Anal. 10 (5), 786–798. doi:10.1016/j.media.2006.07.003.

Desikan, R.S., Ségonne, F., Fischl, B., Quinn, B.T., Dickerson, B.C., Blacker, D., Buckner, R.L., Dale, A.M., Maguire, R.P., Hyman, B.T., Albert, M.S., Killiany, R.J., 2006. An automated labeling system for subdividing the human cerebral cortex on MRI scans into gyral based regions of interest. NeuroImage 31 (3), 968–980. doi:10.1016/j.neuroimage.2006.01.021.

Desmond, J.E., Sum, J.M., Wagner, A.D., Demb, J.B., Shear, P.K., Glover, G.H., Gabrieli, J.D.E., Morrell, M.J., 1995. Functional MRI measurement of language lateralization in Wada-tested patients. Brain 118 (6), 1411–1419. doi:10.1093/brain/118.6.1411.

Dick, A.S., Bernal, B., Tremblay, P., 2014. The language connectome: New pathways, new concepts. Neuroscientist 20 (5), 453–467. doi:10.1177/1073858413513502.

Dick, A.S., Garic, D., Graziano, P., Tremblay, P., 2019. The frontal aslant tract (FAT) and its role in speech, language and executive function. Cortex; a journal devoted to the study of the nervous system and behavior 111, 148–163. doi:10.1016/j.cortex.2018.10.015.

Ferpozzi, V., Fornia, L., Montagna, M., Siodambro, C., Castellano, A., Borroni, P., Riva, M., Rossi, M., Pessina, F., Bello, L., Cerri, G., 2018. Broca's area as a pre-articulatory phonetic encoder: Gating the motor program. Front. Hum. Neurosci. 12 (February), 1–17. doi:10.3389/fnhum.2018.00064.

Fischl, B., van der Kouwe, A., Destrieux, C., Halgren, E., Ségonne, F., Salat, D.H., Busa, E., Seidman, L.J., Goldstein, J., Kennedy, D., Caviness, V., Makris, N., Rosen, B., Dale, A.M., 2004. Automatically parcellating the human cerebral cortex. Cereb. Cortex 14 (1), 11–22. doi:10.1093/cercor/bhg087.

Jeurissen, B., Tournier, J.D., Dhollander, T., Connelly, A., Sijbers, J., 2014. Multi-tissue constrained spherical deconvolution for improved analysis of multi-shell diffusion MRI data. NeuroImage 103, 411–426. doi:10.1016/j.neuroimage.2014.07.061.

Jones, D.K., Cercignani, M., 2010. Twenty-five pitfalls in the analysis of diffusion MRI data. NMR in biomedicine 23 (7), 803–820. doi:10.1002/nbm.1543.

Jones, D.K., Travis, A.R., Eden, G., Pierpaoli, C., Basser, P.J., 2005. PASTA: pointwise assessment of streamline tractography attributes. Magn, Resonanc, Med, 53 (6), 1462–1467. doi:10.1002/mrm.20484.

Kinoshita, M., de Champfleur, N.M., Deverdun, J., Moritz-Gasser, S., Herbet, G., Duffau, H., 2014. Role of fronto-striatal tract and frontal aslant tract in movement and speech: an axonal mapping study. Brain Struct Funct 220 (6), 3399–3412. doi:10.1007/s00429-014-0863-0.

Klingler, J., Ludwig, E., 1956. Atlas cerebri humani: the inner structure of the brain demonstrated on the basis of macroscopical preparations. J. Am. Med. Assoc. 162 (17), 1580. doi:10.1001/jama.1956.02970340070025.

Kong, X.-Z., Mathias, S.R., Guadalupe, T., ENIGMA Laterality Working Group, Glahn, D.C., Franke, B., Crivello, F., Tzourio-Mazoyer, N., Fisher, S.E., Thompson, P.M., Francks, C., 2018. Mapping cortical brain asymmetry in 17,141 healthy individuals worldwide via the ENIGMA Consortium. Proc. Natl. Acad. Sci. USA 115 (22), E5154–E5163. doi:10.1073/pnas.1718418115.

Krainik, A., Duffau, H., Capelle, L., Cornu, P., Boch, A.-L., Mangin, J.-F., Le Bihan, D., Marsault, C., Chiras, J., Lehéricy, S., 2004. Role of the healthy hemisphere in recovery after resection of the supplementary motor area.. Neurology 62 (8). doi:10.1212/01.wnl.0000120547.83482.b1. 1323–32

Kronfeld-Duenias, V., Amir, O., Ezrati-Vinacour, R., Civier, O., Ben-Shachar, M., 2014. The frontal aslant tract underlies speech fluency in persistent developmental stuttering. Brain Struct Funct doi:10.1007/s00429-014-0912-8.

Lehéricy, S., Ducros, M., Krainik, A., Francois, C., Van De Moortele, P.F., Ugurbil, K., Kim, D.S., 2004. 3-D diffusion tensor axonal tracking shows distinct SMA and pre-SMA projections to the human striatum. Cereb. Cortex 14 (12), 1302–1309. doi:10.1093/cercor/bhh091.

Mandelli, M.L., Vilaplana, E., Brown, J.A., Hubbard, H.I., Binney, R.J., Attygalle, S., Santos-Santos, M.A., Miller, Z.A., Pakvasa, M., Henry, M.L., Rosen, H.J., Henry, R.G., Rabinovici, G.D., Miller, B.L., Seeley, W.W., Gorno-Tempini, M.L., 2016. Healthy brain connectivity predicts atrohpy progression in non-fluent variant of primary progressive aphasia. Brain 139 (10), 1–14. doi:10.1093/brain/aww195.

Martínez-Heras, E., Varriano, F., Prčkovska, V., Laredo, C., Andorrà, M., Martínez-Lapiscina, E.H., Calvo, A., Lampert, E., Villoslada, P., Saiz, A., Prats-Galino, A., Llufriu, S., 2015. Improved framework for tractography reconstruction of the optic radiation. PLoS ONE 10 (9), e0137064. doi:10.1371/journal.pone.0137064.

Pedregosa, F., Varoquaux, G., Gramfort, A., Michel, V., Thirion, B., Grisel, O., Blondel, M., Prettenhofer, P., Weiss, R., Dubourg, V., Vanderplas, J., Passos, A., Cournapeau, D., Brucher, M., Perrot, M., Duchesnay, É., 2012. Scikit-learn: machine learning in python. J. Mach. Learn. Res. 12, 2825–2830. doi:10.1007/s13398-014-0173-7.2.

Picard, N., Strick, P.L., 1996. Motor areas of the medial wall: a review of their location and functional activation. Cereb. Cortex 6 (3), 342–353. doi:10.1093/cercor/6.3.342.

Picard, N., Strick, P.L., 2001. Imaging the premotor areas. Curr. Opin. Neurobiol. 11 (6), 663–672. doi:10.1016/S0959-4388(01)00266-5.

Rojkova, K., Volle, E., Urbanski, M., Humbert, F., Dell'Acqua, F., Thiebaut de Schotten, M., 2016. Atlasing the frontal lobe connections and their variability due to age and education: a spherical deconvolution tractography study. Brain Struct. Funct. 221 (3), 1751–1766. doi:10.1007/s00429-015-1001-3.

Ruan, J., Bludau, S., Palomero-Gallagher, N., Caspers, S., Mohlberg, H., Eickhoff, S.B., Seitz, R.J., Amunts, K., 2018. Cytoarchitecture, probability maps, and functions of the human supplementary and pre-supplementary motor areas. Brain Struct. Funct. 223 (9), 4169–4186. doi:10.1007/s00429-018-1738-6.

Smith, R.E., Tournier, J.-d., Calamante, F., Connelly, A., 2012. Anatomically-constrained tractography: improved diffusion MRI streamlines tractography through effective use of anatomical information.. NeuroImage 62 (3). doi:10.1016/j.neuroimage.2012.06.005. 1924–38

Sotiropoulos, S.N., Hernández-Fernández, M., Vu, A.T., Andersson, J.L., Moeller, S., Yacoub, E., Lenglet, C., Ugurbil, K., Behrens, T.E.J., Jbabdi, S., 2016. Fusion in diffusion MRI for improved fibre orientation estimation: an application to the 3T and 7T data of the human connectome project.. NeuroImage 134, 396–409. doi:10.1016/j.neuroimage.2016.04.014.

Sotiropoulos, S.N., Jbabdi, S., Xu, J., Andersson, J.L., Moeller, S., Auerbach, E.J., Glasser, M.F., Hernandez, M., Sapiro, G., Jenkinson, M., Feinberg, D.A., Yacoub, E., Lenglet, C., Essen, D.C.V., Ugurbil, K., Behrens, T.E., 2013. Advances in diffusion MRI acquisition and processing in the human connectome project. NeuroImage 80, 125–143. doi:10.1016/j.neuroimage.2013.05.057. Mapping the Connectome

Tournier, J.-D., Smith, R., Raffelt, D., Tabbara, R., Dhollander, T., Pietsch, M., Christiaens, D., Jeurissen, B., Yeh, C.-H., Connelly, A., 2019. MRtrix3: a fast, flexible and open software framework for medical image processing and visualisation. NeuroImage 202 (January), 116137. doi:10.1016/j.neuroimage.2019.116137.

Van Rossum, G., Drake, F. L., 2012. The Python Language Reference Release 3.2.3, 121.

Varriano, F., Pascual-Diaz, S., Prats-Galino, A., 2018. When the FAT goes wide: right extended frontal aslant tract volume predicts performance on working memory tasks in healthy humans.. PloS One 13 (8), e0200786. doi:10.1371/journal.pone.0200786.

Varriano, F., Pascual-Diaz, S., Prats-Galino, A., 2020. Distinct components in the right extended frontal aslant tract mediate language and working memory performance: a tractography-informed vbm study. Front. Neuroanat. 14, 21. doi:10.3389/fnana.2020.00021.

Vassal, F., Boutet, C., Lemaire, J.J., Nuti, C., 2014. New insights into the functional significance of the frontal aslant tract: an anatomo-functional study using intraoperative electrical stimulations combined with diffusion tensor imaging-based fiber tracking. Br. J. Neurosurg. 28 (5), 685–687. doi:10.3109/02688697.2014.889810.

Vu, A.T., Auerbach, E., Lenglet, C., Moeller, S., Sotiropoulos, S.N., Jbabdi, S., Andersson, J., Yacoub, E., Ugurbil, K., 2015. High resolution whole brain diffusion imaging at 7T for the human connectome project. NeuroImage 122, 318–331. doi:10.1016/j.neuroimage.2015.08.004.

Yeatman, J.D., Dougherty, R.F., Myall, N.J., Wandell, B.A., Feldman, H.M., 2012. Tract profiles of white matter properties: automating fiber-tract quantification. PLoS ONE 7 (11), e49790. doi:10.1371/journal.pone.0049790.